Perez-Cota, Fernando and Smith, Richard J. and Moradi, Emilia and Marques, Leonel and Webb, Kevin F. and Clark, Matt (2015) Thin-film optoacoustic transducers for the subcellular Brillouin oscillation imaging of individual biological cells. Applied Optics, 54 (28). pp. 8388-8398. ISSN 2155-3165

Thin-film opto-acoustic transducers for the sub-cellular Brillouin oscillations imaging of individual biological cells

Fernando Perez-Cota,[1,*] Richard J. Smith,[1] Emilia Moradi,[1,2] Leonel Marques,[1] Kevin F. Webb[1,2] and Matt Clark[1]

[1]*Electrical Systems and Optics Research Division, University of Nottingham, University Park, Nottingham, UK*

[2]*Institute of Biophysics, Imaging and Optical Science (IBIOS), University of Nottingham, University Park, UK*

[*]*eexfap@nottingham.ac.uk*

Abstract: Mechanical characterisation and imaging of biological tissue has piqued interest in the applicability to cell and tissue biology. One method, based on detection of Brillouin oscillations, has already lead to demonstrations on biological cells using ultrasound in the GHz range. In this paper we present a technique to extend this picosecond laser ultrasound technique from point measurements and line scans into high resolution acoustic imaging. Our technique uses a three layered metal-dielectric-metal film under the cell as a transducer for the generation of ultrasound. The design of this transducer and measuring system is optimised to address a limiting SNR factor related to the cell fragility; its sensitivity to laser light. Our approach shields the cell from laser radiation while having acoustic generation, optical detection and aiding heat dissipation. For that, Brillouin detection is performed in transmission rather than reflection. The conditions necessary to perform successfully this kind of detection are discussed and experimental results on phantom, fixed and living cells are presented.

References and links

1. J. W. Lichtman and J. A. Conchello, "Fluorescence microscopy," Nat. Methods **2**, (12), 910–9 (2005).
2. F. Zernike, "Phase contrast, a new method for the microscopic observation of transparent objects part II," Physica **9**, (10), 974–986 (1942).
3. J. Litniewski and J. Bereiter-Hahn, "Measurements of cells in culture by scanning acoustic microscopy," J. Microsc. **158**, (1), 95–107 (1990).
4. M. Lekka, J. Lekki, M. Marszaek, P. Golonka, Z. Stachura, B. Cleff and A.Z. Hrynkiewicz, "Local elastic properties of cells studied by SFM," Appl. Surf. Sci. **141**, (3-4), 345–349 (1999).
5. D. P. Theret. "Application of the Micropipette Technique to the Measurement of Cultured Porcine Aortic Endothelial Cell Viscoelastic Properties," J. Biomech. Eng. **112**, (3) 263 (2008).
6. S. Nawaz, P. Sánchez, K. Bodensiek, S. Li, M. Simons and S. Iwan, "Cell visco-elasticity measured with AFM and optical trapping at sub-micrometer deformations," PloS one **7**, (9) e45297 (2012).
7. J. A. Hildebrand, D. Rugar, R. N. Johnston, and C. F. Quate. "Acoustic microscopy of living cells," Proc. Natl. Acad. Sci. **78**, (3), 1656–60 (1981).
8. T. Kundu, J. Bereiter-Hahn, and K. Hillmann, "Measuring elastic properties of cells by evaluation of scanning acoustic microscopy V(Z) values using simplex algorithm," Biophys. J. **59**, (6), 1194–1207 (1991).
9. T. Kundu, J. Bereiter-Hahn, and I. Karl. "Cell property determination from the acoustic microscope generated voltage versus frequency curves," Biophys. J. **78**, (5), 2270–9 (2000).
10. J. Heiserman. "Cryogenic acoustic microscopy," J. Acout. Soc. Am. **67**, (5), 1629 (1980).
11. M. S. Muha, A. A. Moulthrop, G. C. Kozlowski, and B. Hadimioglu. "Acoustic microscopy at 15.3 GHz in pressurized superfluid helium," Appl. Phys. Lett. **56**, (11) 1019 (1990).

12. B.Hadimioglu, "Water acoustic microscopy at suboptical wavelengths," Appl. Phys. Lett. **43**, (11), 1006 (1983).
13. P. A. Mante, J. F. Robillard, and A. Devos, "Complete thin film mechanical characterization using picosecond ultrasonics and nanostructured transducers: experimental demonstration on SiO[sub 2]," Appl. Phys. Lett. **93**, (7) 071909 (2008).
14. P. Babilotte, P. Ruello, D. Mounier, T. Pezeril, G. Vaudel, M. Edely, J-M. Breteau, V. Gusev, and K. Blary, "Femtosecond laser generation and detection of high-frequency acoustic phonons in GaAs semiconductors," Phys. Rev. C **81**, (24), 245207 (2010).
15. W. Chen, Y. Lu, H. Maris, and G. Xiao, "Picosecond ultrasonic study of localized phonon surface modes in Al/Ag superlattices," Phys. Rev. C **50**, (19), 14506–14515 (1994).
16. O. Wright, B. Perrin, O. Matsuda, and V. Gusev, "Optical excitation and detection of picosecond acoustic pulses in liquid mercury," Phys. Rev. C **78**, (2), 024303 (2008).
17. M. Ducousso, O. E.-F. Zouani, C. Chanseau, C. Chollet, C. Rossignol, B. Audoin, and M.C. Durrieu. "Evaluation of mechanical properties of fixed bone cells with sub-micrometer thickness by picosecond ultrasonics," Eur.Phys.J.-Appl Phys. **61**, (1) 11201 (2013).
18. T. Dehoux and B. Audoin, "Non-invasive optoacoustic probing of the density and stiffness of single biological cells," Appl. Phys. **112**, (12), 124702 (2012).
19. G. Scarcelli, P. Kim and S. H. Yun, "In vivo neasurement of age-related stiffening in the crystalline lens by Brillouin optical microscopy," Biophys J. **101**, (6), 1539–1545, (2011).
20. G. Scarcelli and S. H. Yun, "Confocal Brillouin microscopy for three-dimensional mechanical imaging," Nat. Photonics **6**, 39–43, (2008).
21. C. Thomsen, H.T. Grahn, H.J. Maris, and J. Tauc, "Picosecond interferometric technique for study of phonons in the brillouin frequency range," Opt. Commun. **60**, (1), 55–58 (1986).
22. C. Rossignol, N. Chigarev, M. Ducousso, B. Audoin, G. Forget, F. Guillemot, and M. C. Durrieu, "In Vitro picosecond ultrasonics in a single cell," Appl. Phys. Lett. **93**, (12), 123901 (2008).
23. B. Audoin A. Gadalla, T. Dehoux, "Tranverse mechanical properties of cel walls of single living plant cells probed by laser-generated acoustic waves," Planta **239**, 1129–1137, (2014).
24. L. G. Garretón, B. Audoin, C. Rossignol, N. Chigarev, M. Ducousso, G. Forget, F. Guillemot and M. C. Durrieu, "Picosecond acoustics in vegetal cells: non invasive in vitro measurements at a sub-cell scale," Phys. Proc. **3**, (1), 323–331 (2010).
25. P. A. Elzinga, F. E. Lytle, Y. Jian, G. B. King, and N. M. Laurendeau, "Pump/Probe Spectroscopy by Asynchronous Optical Sampling," Appl. Spec. **41**, (1), 2–4 (1987).
26. R. J. Smith, F. Perez-Cota, L. Marques, X. Chen, A. Arca, K. Webb, J. Aylott, M. G. Somekh, and M. Clark, "Optically excited nanoscale ultrasonic transducers," J. Acoust. Soc. Am. **137**(1), 219–227 (2015).
27. M. O. Culjat, D. Goldenberg, P. Tewari, and R. S. Singh, "A review of tissue substitutes for ultrasound imaging," Ultrasound Med. Biol. **36**,(6), 861–73, (2010).
28. M. Xiaoyan, J. Q. Lu, R. S. Brock, K. M. Jacobs, P. Yang, and X. H. Hu, "Determination of complex refractive index of polystyrene microspheres from 370 to 1610 nm," Phys. Med. Biol. **48**, (24), 4165 (2003).
29. D. M. Smith and T. A. Wiggins, "Sound speeds and laser induced damage in polystyrene," Appl. Opt. **11**, (11), 2680–2683 (1972).
30. S. Tornaletti and G. P. Pfeifer, "UV damage and repair mechanisms in mammalian cells," BioEssays **18**, (3), 221–8 (1996).
31. F. Lanni, A. S. Waggoner, and D. L. Taylor, "Structural organization of interphase 3T3 fibroblasts studied by total internal reflection fluorescence microscopy," J. Cell Biol. **100**, (4), 1091–102 (1985).
32. R. J. Smith, R. A. Light, S. D. Sharples, N. S. Johnston, M. C. Pitter, and M. G. Somekh, "Multichannel, time-resolved picosecond laser ultrasound imaging and spectroscopy with custom complementary metal-oxide-semiconductor detector," Rev. Sci. Instrum. **81**, (2), 024901 (2010).
33. E. Weiss, P. Anastasiadis, G. Pilarczyk, R. Lemor, and P. Zinin, "Mechanical Properties of Single Cells by High-Frequency Time-Resolved Acoustic Microscopy," IEEE Trans. Ultrason., Ferrelect., Freq. Control **54**, (11), 2257–2271 (2007).

1. Introduction

Ultrasonics offers an attractive route to high resolution imaging and measurement. The speed of sound is typically five orders of magnitude lower than the speed of light and, at the same wavelength, ultrasound frequencies are in the GHz range. At these frequencies and above, ultrasound therefore has the potential to provide higher resolution imaging than optical microscopy. Furthermore, many small-scale biological objects, such as cells, exhibit very little intrinsic optical contrast, requiring preparation such as staining with fluorophores [1] or the deliberate introduction of useful artefacts in the aperture plane which translate phase contrast within the sample into amplitude contrast at the imaging plane [2] . Recent work has suggested

that the strongly-varying mechanical properties in these structures may offer further useful contrast in the ultrasound regime [3–6], however the choice of high resolution and *non-destructive* mechanical imaging techniques for the study of living biological specimens is remarkably limited. Access to this kind of tool could aid the study of cell processes such as mitosis, migration, force production, mechanosensitivity, and address the myriad dynamic events which underlie the directed stance of living cells towards their environment.

Acoustical methods for the imaging and characterisation of biological tissue has a noble history at the macroscopic scale, and has lead to an explosion of knowledge in the fields of obstetrics, cardiology, gastrointestinal and abdominal surgery, and has been of diverse utility in the research as well as clinical arena. Ultrasound is non-invasive, requires little sample preparation and is relatively cheap. The potential for a new imaging technique with sub-optical resolution has inspired much research in GHz ultrasonics, for example, the scanning acoustic microscope (SAM) has been used for non-destructive acoustic imaging of biological cells [7]. It showed promise as a high resolution method of performing acoustic imaging and mechanical characterisation with minimal impact on cultured cells [3, 8, 9]. However, this implementation is practically difficult at the frequencies required to image the internal structure of most cells. Typically those systems are restricted to the 1-2GHz range, which limits their resolution below of that of optical microscopes. This has previously been overcome by using cryogenic couplants, such as liquid argon [10] or liquid helium [11], but these approaches are not applicable to living cells, while the low temperature has the potential to affect the acoustic properties of the cell.

There are significant practical problems to increase the frequency of ultrasound above the 1GHz region using the piezoelectric transducers commonly found on acoustic microscopes. For instance, the attenuation of ultrasound is very high in the GHz region (1900dBmm^{-1} at 4.4GHz [12]), which introduces impedance-matching issues and restricts the use of couplants. The small size of the transducers required at multi-GHz frequencies further imposes a considerable technical challenge to provide electrical wiring to the transducer. Moreover, the electronics to drive and detect the multi-GHz analogue signals are expensive and difficult to work with.

Using picosecond laser ultrasonics it is possible to overcome some of the limitations of piezoelectric-based systems. Here, short pulsed lasers are used to generate and detect the ultrasound. With this arrangement some of the practical problems associated with piezoelectric transducers are overcome. By abrogating the need for a couplant, lasers provide access to very high frequencies, while the pump-probe architecture removes the need for extremely fast electronics and detectors. Picosecond laser ultrasound has been used to investigate optical and mechanical properties of thin films [13], semi-conductors [14], novel materials [15], liquids [16], and other samples. Recently, picosecond laser ultrasound (PLU) has been applied to measure the mechanical properties of cells [17, 18]. The method uses Brillouin oscillations to detect a sound wave travelling through a cell in order to evaluate its viscoelastic properties.

There is discussion in the literature about the differences of mechanical properties obtained at GHz range [19]. Whether these properties obtained at high frequencies are good approximations to standard values or not, the opto-mechanical nature of the measurements it is still a useful contrast mechanism for imaging as well as source for quantitative measurements of the refractive index and the speed of sound [17–20].

Brillouin oscillations are a PLU way of detecting time-resolved Brillouin scattering. It is the result of the interference between Brillouin scattering and a reference beam [21]. The change in pressure produced by a laser-induced soundwave introduces a local refractive index modulation that creates an interface at which light is scattered. If scattered light interferes with the source, then Brillouin oscillations are observed (see Fig. 1). The dependence of this oscillation to the speed of sound and refractive index is given by:

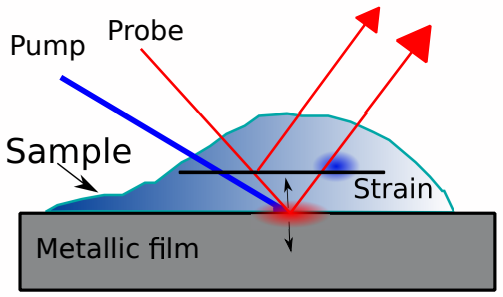

Fig. 1: Conventional Brillouin detection on a Biological cell. The probe beam is split by the acoustic wavefront due to acousto-optic interactions, and then the two beams interfere, giving rise to Brillouin oscillations. The cell under interrogation is exposed to both laser beams, and to the heat generated in the strain generation process.

$$f_B = \frac{2n\nu}{\lambda}\cos\theta \tag{1}$$

where ν is the speed of sound, n the refractive index, λ the probing light wavelength and θ the incidence angle. The Brillouin frequency will depend then on the material characteristics and probing light wavelength. The method can probe at a wide range of frequencies in the GHz regime (typically 5-20GHz in physiological media) and by raster-scanning point by point, can produce images with a lateral resolution limited by the optical spot sizes of the lasers, and a depth resolution limited by the acoustical wavelength.

Brillouin scattering detection has been demonstrated in individual living onion cells [22]. In that work, different Brillouin frequencies are measured for the vacuole and nucleus which suggests there is good acoustical contrast within the cell. An alternative configuration was applied to prevent laser and heat damage with a trade off in signal-to-noise ratio (SNR) and experimental simplicity [18]. More recently, an increase in resolution was demonstrated by use of a shorter probe wavelength [17], where measurements of the thickness of sub-micrometer fixed bone cells were performed. The technique has been also used to study inner structure of onion cell walls [23]. The viability of this technique for living cells in terms of laser exposure and temperature rise was analysed, concluding it is in principle biocompatible [24]. Extensive modelling and fitting has allowed the evaluation of the elastic properties with a 1μm lateral and 0.25μm in-depth resolution [24]. We consider then that Brillouin oscillations have great potential for the acoustic characterisation and imaging of cells, because of the non destructive nature of ultrasound and the high frequencies of the Brillouin oscillations. However, this technique has not yet been successfully applied to the production of images, and clearly requires significant optimisation for applicability in living preparations of mammalian cells.

Brillouin scattering detection in the form of confocal Brillouin microscopy has also been reported [19,20]. These techniques, which are also capable of measuring the Brillouin frequency, do not resolve the signals in time and hence only the relative weights of the Brillouin components can be measured. By detecting Brillouin oscillations using PLU and resolving the signals in time, it is possible to increase scattered light by the generation strong acoustic fields and to locate the Brillouin components both temporally and spatially with the acoustic wavelength greatly reducing the measurement volume. This in turn allows the potential for three dimen-

sional imaging. However, the time-resolved capability of PLU implies the use of pulsed lasers and complicated detection schemes.

There are many types of biological preparation which appear suitable for Brillouin oscillations imaging. Thin cells (1-10μm) with a lateral size of microns are ideal subjects for the technique since they are well matched to the lateral resolution (optical) and acoustic penetration depth (5-10μm). However, there are technical challenges to be addressed in order to apply Brillouin oscillation imaging to biological cells. Picosecond laser ultrasound is based on the pump-probe technique, which typically uses a mechanical delay line to resolve in time the very fast GHz events. This approach is however slow for the purposes of this work exposing unnecessarily the specimens for long periods of time. The SNR in picosecond ultrasound experiments is usually low and the amount of laser power that can be used before damaging a cell is limited so additional averaging might be required which is also time consuming.

This paper further introduces and characterises a novel implementation of an optically-driven, three-layer, thin-film ultrasonic transducer [26] for detection of Brillouin oscillations in the transmission path. This application provides optically-selective shielding from the UV pump beam, transmits the red probe, generates acoustic waves and aids to dissipate heat. It is also surface-functionalised to allow the attachment and normal growth of a variety of biological cells. This approach in conjunction with a fast ASOPS pump and probe system [25] allows imaging of the Brillouin oscillation frequency. The optical (§2.1), and mechanical (§2.2) designs, operation and design criteria to achieve the desired transmission performance are described in §2. A description of the experimental setup is presented in §3.1, followed by results obtained from cellular phantoms, fixed cells, and living cultures of mouse-derived fibroblasts (3T3 immortalised cell line §3). Finally, the significance of our work and its direction of travel in the field is discussed (§4).

2. Design of thin-film opto-acoustic transducers for Brillouin detection in transmission

In this paper, an opto-acoustic transducers is used to generate ultrasound. These transducers consist of a three-layered thin-film structure of metal-dielectric-metal, in this case gold as the metal and indium tin oxide (ITO) as the dielectric (see Fig. 4). These sensors were initially designed as high-frequency nano-scaled ultrasonic sources/detectors [26]. Here they are re-engineered to serve in the production of Brillouin oscillation frequency images. They strongly absorb at one wavelength of light (λ_{pump}) and reflect/transmit at a second wavelength (λ_{probe}), which allows flexibility of design. The transducers form a simple plate structure which will resonate mechanically when excited and, if in contact with another medium, radiate acoustic waves.

For our experiments, the two optical wavelengths (390nm at λ_{pump} and 780nm at λ_{probe}) are determined by our laser system which governs the choice of materials and layer thicknesses. However, as can be seen in §2.1 and §2.2, there are a large range of possible layer thicknesses that can be used to allow some degree of freedom with which to tune the transmission and other characteristics.

Detection using light transmitted by the transducer is a critical design feature, as we are simultaneously exploiting the transducer itself to act as a shield and protect the specimen from pulsed laser light. In order to make that possible, it is necessary to tune the transducer layer thicknesses to reach high transmittance at λ_{probe} without compromising absorption at λ_{pump}. Optical and mechanical models were used to understand the viability of this approach.

2.1. Optical Characterisation of the transducers

The devices operate in a manner similar to that of a zero-order Fabry-Pérot interferometer. The layer structure is designed so that the top and bottom metal layers are partial reflectors.

Part of the probe beam incident on the transducer is resonantly reflected and transmitted by the structure. The transducer exhibits sensitivity to incoming waves and to its own mechanical resonance. The magnitude of the sensitivity depends on the layer thicknesses [26]. The model used for these devices is based on the calculation of the Fresnel coefficients which assumes the structure is of infinite lateral width; a fair approximation provided the width of the illumination is several times the optical wavelength.

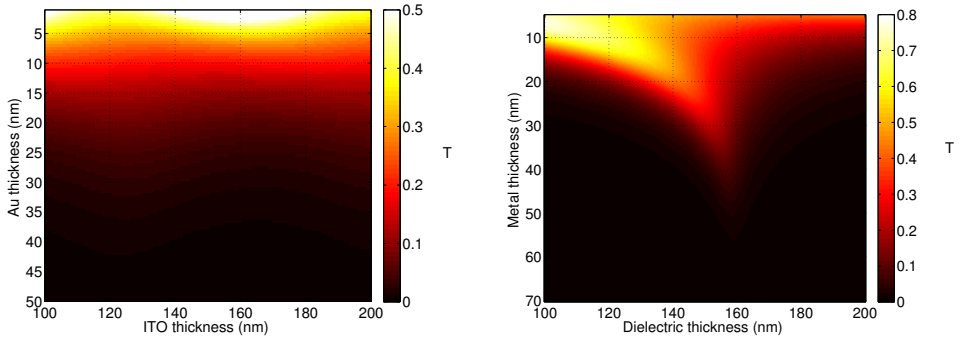

(a) (b)

Fig. 2: Optical model of the transducers in transmission. (a) Pump transmittance. (b) Probe transmittance.

The model calculates the transmission and absorption for λ_{pump} as well as transmission and sensitivity of λ_{probe} to the transducer size [26]. In the model, the top and bottom gold layers of the transducer are assumed to have the same thickness which varies from 5 to 60nm and the ITO layer thickness changes from 100 to 200nm. Figure 2, shows the results of the optical models for transmission. It is possible to see in Fig. 2(a) that above 12 nm of gold, transmittance of λ_{pump} is low. For device dimensions of ITO between 140 and 160nm and gold layers of 20nm, it is possible to have transmittance for λ_{probe} up to 40% around the transmission peak [see Fig. 2(b)]. The transducer absorption for λ_{pump} has no significant variation across the range and the sensitivity to incoming waves of the transmitted beam is approximately half of that in the reflected case, as previously reported (not shown) [26].

2.2. Mechanical Characterization of the transducers

The most important constraint in choosing the layer thicknesses is meeting the optimal conditions for generation and detection. We modelled the structures to determine their expected resonance frequencies and the amplitude at the Brillouin frequencies we expect from a cell (between 5 and 6GHz) [22].

Since the structures have a number of boundaries and the excitation is performed thermoelastically using an optical source, modelling of the vibration does not lend itself to easy analytical analysis. Instead, we have modelled these devices using finite element modelling (FEM) [26] and used a coupled optical-thermal-mechanical model to predict their behavior when excited by a short laser pulse. The FEM model obtains the excitation of the pump pulse as an injection of heat into the metal layers. The model then computes the temperature changes, stress and motion of the structure. Since these devices are large plates (25mm diameter) excited with a laser spot at least several times the thickness of the transducers, the devices presented here can be adequately modelled using simple 1D approximations.

The output of the model, which consists of time traces of the displacement of the metal layers, helps to evaluate the resonance frequency as well as the generated acoustic amplitude at

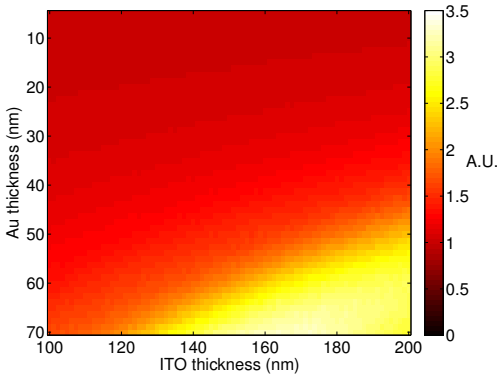

Fig. 3: Simulated amplitude generated by the transducer at 5.5GHz for different layer thicknesses. Amplitude is uniform, except when the resonance of the transducer overlaps 5.5GHz [26].

5.5GHz (which is the centre of the expected Brillouin oscillation frequencies from a cell). Figure 3 shows the amplitude at 5.5GHz calculated from the output of the model, revealing small amplitude change over the range of layer thicknesses. This gradient will affect the amplitudes of the measured Brillouin signals, however it has little or no effect on their frequency. For the thicker devices, the amplitude is observed to increase rapidly. This rise in amplitude is due to the resonance reaching 5.5GHz. However, we choose to use the tail of the transducer response to simplify data post-processing and to keep transmission at λ_{probe} high.

The resonance frequencies for a similar range of device sizes as shown in Fig. 3 are presented in Smith *et al* [26]. The frequencies evaluated from the simulations there vary from 5 to 19 GHz. The model also produces the temperature profile on the layers. From there, a reduction of $\sim$50% of the instantaneous temperature rise induced by the pump pulse was seen from the surface absorbing the pump laser to the one where the cell is.

2.3. Transmission detection and design criteria

In Fig. 4, the configuration for detection in transmission is shown: lasers are incident to the transducer through the substrate. The transducer is tuned for high transmittance for λ_{probe} while transmittance remains low at λ_{pump} due to the high absorption of gold (pump beam not shown for clarity). The high transmission at λ_{probe} allows transmitted detection while high absorption at λ_{pump} produces strain pulses efficiently. Additionally, the substrate helps to dissipate heat.

To allow high λ_{probe} transmission, the thicknesses of the layers are chosen so that the transmittance of the transducer sits around the top of the optically resonant transmission peak[see Fig. 2(b)]. Due to high transmittance of the transducer, a second Brillouin signal will be detected from the substrate (see Fig. 4). Since the substrate is considerably stiffer than any biological cell, the detected Brillouin frequency coming from the scattered light on it will be considerably higher (22GHz for glass). The mechanical resonance of the transducer will also be detected. This signal can be handled in the post-processing since: it typically decays five times faster than the Brillouin signals and its frequency is round twice the frequency we expect from the cells. The different components in the detected signals are then in different bands, facilitating spectral separation by filtering.

In our approach, the intensity of λ_{probe} and λ_{pump} seen by the cell is reduced by up to 60% and 90% respectively (see figure 2). This allows to increase laser power and hence SNR. In a conventional reflection mode time-resolved measurement (see figure 1), the cell receives the

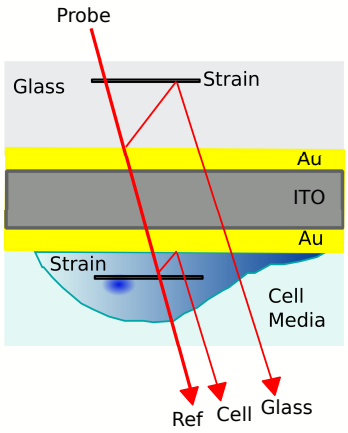

Fig. 4: Schematic of Brillouin detection in transmission using a thin-film transducer. This configuration prevents over-exposure of the specimen to laser beams for delicate subjects such as biological cells. Two Brillouin signals are detected; one from the specimen(ref+cell) and one from the substrate (ref+glass). The dimensions of the transducer are exaggerated and beams are shown at an angle for clarity.

whole of the light intensity but only part of the probe beam reaches the detector due to losses in the many optical elements. The improvement of the SNR, along with the reduction of the instantaneous temperature rise at the cell/transducer interface, allows imaging without compromising the integrity of the examined cell. This approach also simplifies the detection set-up, as there is no need to separate laser light travelling in opposite directions.

From our models, we expect that a transducer with dimensions of 20+/-5nm of gold in both top and bottom layers and 145+/-15nm of ITO in the middle will be suitable for transmittance detection. It will have a resonant frequency of 9-11Ghz which is easy to separate in the frequency domain from the Brillouin frequency of a cell. A 0.25-0.4 transmittance for λ_{probe} allows a good detection level, with a reduced input power at the sample that is conferred by the experimental setup. For λ_{pump} an approximate 0.4 overall device absorption means good light to sound conversion and a 0.1 transmittance means reduced exposure at the shorter wavelengths that are damaging for biological cells.

3. Experimental results

3.1. Experimental setup

Figure 5 shows a simplified schematic of the experimental system. The experiment is based around a dual laser asynchronous optical sampling (ASOPS) system [25, 26]. This controls two 150 femto-second pulsed lasers with repetition rates of $\sim$100MHz which allows a delay between the pulses to be set and swept electronically at relatively high speed. In our system, the delay repetition rate between the pump and probe pulses is swept from 0ns to 10ns every 100μs corresponding to a 10kHz difference in the repetition rate of the lasers. That means that we can achieve up to 10000 traces per second, provided that the acquisition system is capable of such speeds. This kind of system represents a significant improvement over the conventional mechanical delay line in terms of speed and arrangement simplicity.

The pump laser is doubled in frequency to provide the 390nm pump beam. Both beams are combined and focused together through a 50x long working distance objective. Adjustable mir-

rors and a lens on a manual stage on the pump path allows moving the spot of the pump in order to overlap it accurately to the probe beam in all directions. The probe beam is detected below the sample after being collected by an objective lens (20x) and is focused to a photodiode. The sample is scanned by moving electromechanical stages with a minimum step motion of 100nm taking typically 15000 averages per point which takes ∼4s. For each measurement, the raw trace is processed to remove thermal background and evaluate its Brillouiin frequency. The system uses typical average powers of 1mW in the probe and 0.5mW in the pump corresponding to pulse energies of 10pJ and 5pJ and peak powers of ∼60W and ∼30W respectively. A spectrally-distinct LED source is used to allow brightfield imaging of the sample by a CCD camera.

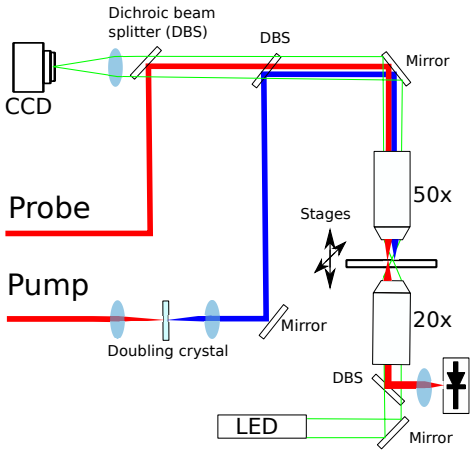

Fig. 5: Experimental setup. Two lasers electronically synchronized by an ASOPS system are combined by dichroic mirrors to be focussed together by a long working distance objective. The probe beam is detected in transmission. An LED is used as a light source to build an optical image of the specimen on the CCD camera.

3.2. Brillouin detection in transmission

Using a sputter coater, transducers were built by depositing the layers in 25mm coverslips in order to test the transmission detection. A spectrometer arrangement was used to measure the thickness of the layers with a +/-2nm accuracy. All tests were performed using the same amount of laser power (0.4mW for λ_{pump} and 4mW for λ_{probe}). The test included simple transmission for both laser wavelengths and then Brillouin scattering detection from a water film. Water was used due to the similarity of its properties to those of cells. With gold layers thickness of 20nm, devices with 100, 120, 140 and 160nm of ITO were fabricated. In Fig. 6, the transmittance for both lasers is measured for the four devices. The continuous line represents the theoretical transmittance whilst the circles the experimental results. There is good agreement on the four devices. This means that the transducers layer thicknesses are modelled correctly confirming the properties of the device.

Figure 7 shows an example of a typical trace and its Fourier transform obtained from a water film on a 20-140-20nm transducer. Two sharp peaks at 5GHz and 22GHz correspond to Brillouin signals from the water and substrate respectively, the broad peak is the resonance of the device. The resonance peak frequency matches the expected value presented on *Smith et al* [26], which is further confirmation of layer thickness and model validity. The probed acoustic

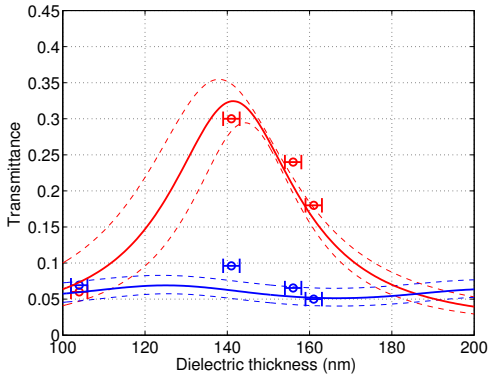

Fig. 6: Transmission of light through the transducer at λ_{pump}(blue) and λ_{probe}(red) for devices with layer thickness of approximately 20nm of gold and 100, 140 155 160nm of ITO. Solid lines represent theoretical calculations and dotted ones deviation for an expected error of -/+ 2nm on gold layer thickness evaluation. Circles represent experimental results taken of samples made by sputtering layers. The horizontal error bars represent thickness evaluation error on the ITO layer.

wave lasts approximately 4ns, which at a sound speed of ∼1550m/s (assuming refractive index 1.33), reaches approximately 6.5 microns into the water. At ∼5GHz the acoustic wavelength is 300nm.

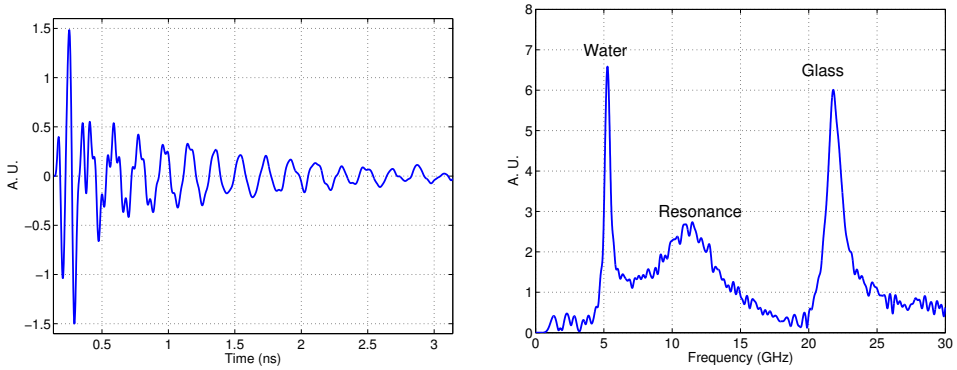

(a) (b)

Fig. 7: Example experimental trace of a picosecond ultrasound experiment using a Au:ITO:Au 20:140:20nm transducer in transmission. (a) Time trace itself. (b) Its Fourier transform where the three frequency components detected are clearly visible; the signal of interest (5GHz), the transducer resonance (11GHz) and the Brillouin frequency from the substrate (22GHz)

It is possible to see from Fig. 7(a) that the Brillouin signal of the glass substrate and the water coexist in time. Those signals are only related temporally and not spatially since they originate in acoustic waves travelling in opposite directions (see Fig. 4).

3.3. Brillouin imaging of a phantom cell

In order to optimise the signals and signal processing against an inert, unchanging sample, we designed and constructed our own cellular-scale phantoms. Phantoms are widely used for sim-

ulation and calibration, and they have many advantages over real samples. They are made of well characterised materials, they have a fixed shape and size and do not change or deteriorate like real cells or tissue. In our case the phantom serve as test/calibration targets for the approach presented in this paper, and to characterise the response of the system to a homogeneous material of known composition. This allows comparison of measured acoustic parameters with those from the literature. There are commercially available materials used specifically for soft tissue phantom fabrication with speeds of sound from 1460-1600m/s [27]. However, those are difficult to use in the scale required for fabrication of phantom cells. Instead, fused polystyrene microspheres were used to build a transparent micro-object with a shape that resembles a biological cell. However, polystyrene has the disadvantage of having significantly faster speed of sound than water.

The phantom cells were fabricated by using 5μm polystyrene microspheres(Bangs Laboratories, Inc) prepared in a diluted solution (1:500). Then the microspheres were dispersed across the transducers surface to prevent large segregation and melted in an oven at 245^{o}C for 30 to 45 minutes. Figure 8 shows an example of these objects before(a) and after(b) the melting process. This process helps to create good contact between phantom and transducer, essential for good acoustic transmission, as well as immobilising these structures for imaging.

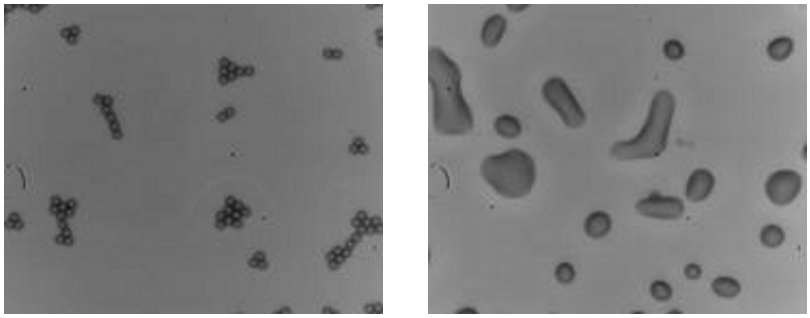

(a) (b)

Fig. 8: Example of PS phantoms used to simulate the shape and scale of a cell. (a) Deposited polystyrene 5μ particles. (b) Particles melted together by heating them at 245 centigrades for 30 to 45 minutes. Particles shown in (a) and (b) are not from the same frame.

By submerging the phantom in water, we simulate the presence of physiological media. The water properties further serves as a background reference for contrast comparison between polystyrene and its surroundings. The sample was mounted in a two-coverslip chamber(Live Cell Instruments Inc. CF-T) with the phantoms facing the detection path objective (20x see Fig. 5) in order to perform detection in transmission. Figure 9 shows a sample trace at one point on the sample. The transition in the polystyrene-water boundary, which marks the time of flight of the acoustic wave inside the phantom, it is clearly observable. The Brillouin oscillation frequencies on polystyrene and water at λ_{probe} are 9 and 5GHz respectively. The significant difference in frequency makes the transition easy to see, however in the case of a real cell the frequency contrast are likely to be much smaller.

Figure 10 shows the result of a scan over a phantom cell. The scan area was 30 by 30 microns with 1 micron steps. The 900 points were acquired in approximately one hour. Figure 10(a) shows an optical picture of the scanned phantom. Here it is still possible to see the shape of the spherical particles used to build it. On Fig. 10(b) the Brillouin frequency map obtained from that picture is shown. The correlation between the optical picture and the acoustic one is good. Contrast is strong and the variation of the Brillouin frequency within the phantom is

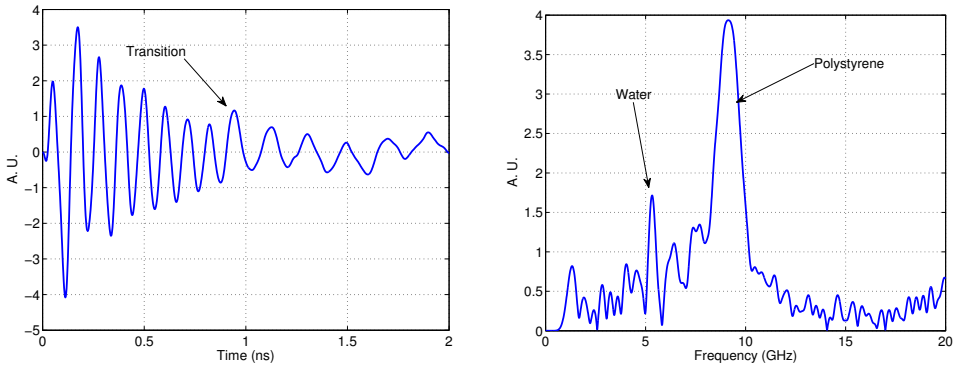

(a) (b)

Fig. 9: Example of transition from polystyrene to water. (a) Time trace. (b) Its Fourier transform. When the soundwave leaves the polystyrene and enters the water there is a change of Brillouin frequency due to change in refractive index and speed of sound.

small, suggesting good homogeneity. Moreover, no correlation was observed for the 22GHz component confirming it is a signal originating in the substrate.

If the refractive index of the phantom is constant, its Brillouin map is directly proportional to the speed of sound. Taking polystyrene refractive index as 1.58 at λ_{probe} [28], water as 1.33 and applying Eq. (1), a speed of sound of map was calculated. The corresponding refractive index of each point was assigned acording to its Brillouin frequency [see Fig. 10(c)]. This result is similar to the bulk speed of 2407m/s reported by *D. M. Smith et al* [29].

3.4. Brillouin imaging on cultured cells

Even though the results above show the viability of the transmission approach on PS phantoms, there are significant additional challenges when it come to addressing real cells. First, the damage thresholds are lower, and depend on the type of cell. While plant cells are rather robust to laser illumination, mammalian cells exhibit considerable sensitivity to high-energy photons in the visible and UV regimes [30]. The Brillouin shift at the cell-media boundary is significantly smaller than seen with the phantoms, which will reduce contrast with the background. The axial thickness of a cell further varies widely from cell to cell, and within single cell, submicron vertical dimensions surrounding cell margin extend to many microns at the centre of mass. Furthermore, the cell is far from being an homogeneous material, containing myriad subcompartments and internal structures. These are worthy targets of investigation, but may make analysis of the resulting Brillouin traces complex. All those points together make our targeting of living mammalian cells a significant challenge.

As an intermediate step we employed fixed 3T3 fibroblast cells, since fixation using paraformaldehyde both mechanically and biochemically stabilises the cell structure, sterilises the preparation, and freezes the action in place to allow extended imaging. Micro and nanoscopic features of the sample are preserved however, successful application of PLU to fixed cells will thus delineate the potential for applicability in more complex and sensitive preparations. 3T3 fibroblast cells were cultured on the transducers for 24hrs using standard culture conditions, prior to fixation in paraformaldehyde(4%) in phosphate-buffered saline (PBS). The fixed cells were kept in PBS during the experiment, allowing gentle flow which prevented air bubble formation.

Figure 11 shows two fixed 3T3 fibroblast cells and the result of a 2D scan of their Brillouin

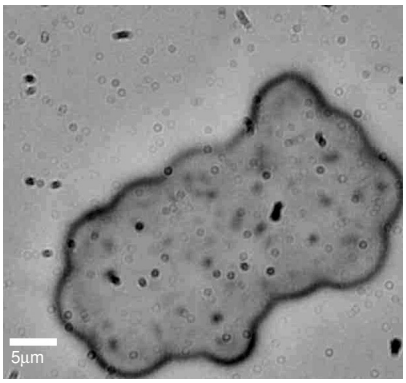

(a)

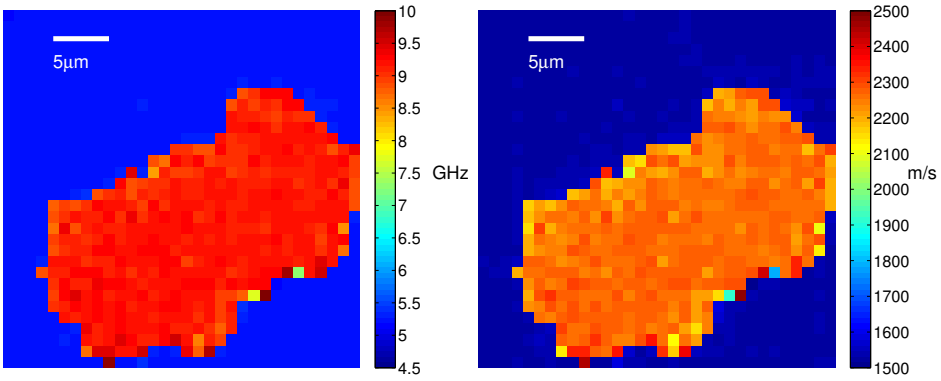

(b) (c)

Fig. 10: Scan over a phantom cell in water. (a) Optical picture of the phantom cell. (b) Its Brillouin map. (c) Its speed of sound map. The speed of sound map is calculated from Eq. (1) assigning the refractive index to each point acording to its Brillouin frequency (for instance, $n_{x,y} = n_{water} \iff f_{Bx,y} \sim$5GHz)

frequency. The scanned area was 60 by 60 microns, with one micron steps. Fig. 11(b) shows the Brillouin oscillation frequencies obtained from this experiment. The correlation between the optical image and the Brillouin map is good. The nucleus of both cells have clearly different Brillouin frequency, which will be due to differences in the local speed of sound and refractive index. This change it is not visible in the optical picture and it is a good example of the potential of mechanical contrast. There are also faint change of Brillouin frequency in the marginal filopodia of the cell which demonstrate the capabilities of our approach to see small Brillouin frequency shifts.

Similar experiments, limited to single lines of Brillouin acquisition, were then performed on living cultures of 3T3 cells in Hanks balanced salts solution (HBSS) supplemented with 4-(2-hydroxyethyl)-1-piperazineethanesulfonic acid (HEPES, 25mM) as a buffer to maintain pH under ambient conditions. Using the same perfused chamber it was possible to keep cells alive, for more than 5 hrs in similar conditions to our experimental setup. The whole experiment was physically enclosed for temperature stability. The average powers for pump and probe were 0.4 and 1mw respectively (the cell will only see 0.04 and 0.3 mW due to the transducer transmittance characteristics as shown in Fig. 2).

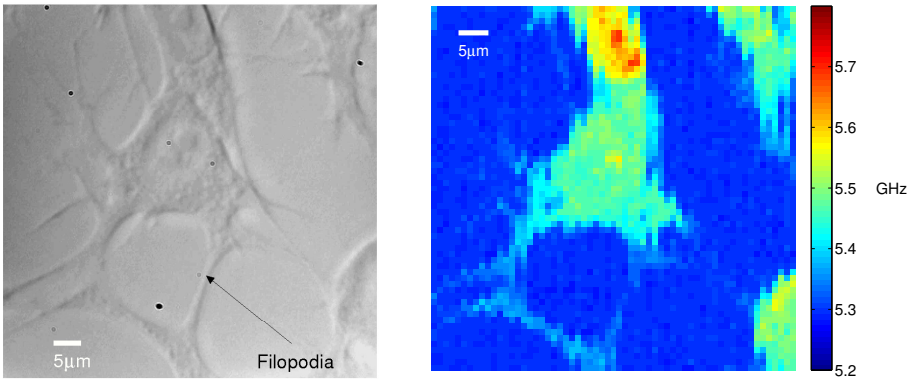

(a) (b)

Fig. 11: Optical image of a 3T3 fixed cell (a) and its Brillouin map obtained using the transmittance approach (b)

Figure 12 shows the result from a living 3T3 cell with an optical picture of the scanned area before and after the scan. The scan was 40x1 microns with one micron steps leading to approximately 3 minutes of scanning time. The resultant Brillouin frequency (d) shows good correlation with the optical picture(a). The B-scan (b) shows clearly the effect of the cell on the phase of the waves. Similar to the fixed cell case, the frequencies are higher in the centre of the cell. If we compare optical images before (a) and after (c) the scan, we can see changes in the cell topology. These changes may represent reaction of the cell to the beam, although the morphology and structural integrity of the cell remains intact.

The Brillouin oscillation frequencies measured on culture cells were between 5.25 and 5.5GHz with 50 and 250MHz shift from the background media. Assuming the refractive index of 1.36 [31], the speed of sound would change from approximately 1548m/s to 1605m/s. Near the edges of the cell the shift is harder to see because the cell is thinner, so the dominant frequency on the Fourier transform will be that of the media as the volume fraction of interaction becomes dominated by media properties.

4. Discussion

4.1. Sectioning and profile extraction

The change in Brillouin frequency presented in this work is an average taken from the measured volume. However, given the acoustic wavelength(300nm); further analysis of the time-resolved data, not demonstrated here, could resolve the position and thickness of features inside the volume along the z axis (if the refractive index is known).This could provide sectioning capabilities with z resolution of the order of half the acoustic wavelength. When a wave is travelling from one media to another, the Brillouin frequency we observe will change due to the different speed of sound and refractive index. If the surrounding media has known characteristics, a known reference frequency will be available to determine when the sound leaves the specimen and enters the media. If we know the refractive index beforehand and the Brillouin frequency from the traces themselves, then the thickness of the object will be given by:

$$h = \frac{\delta t f_B \lambda_{probe}}{2n} \tag{2}$$

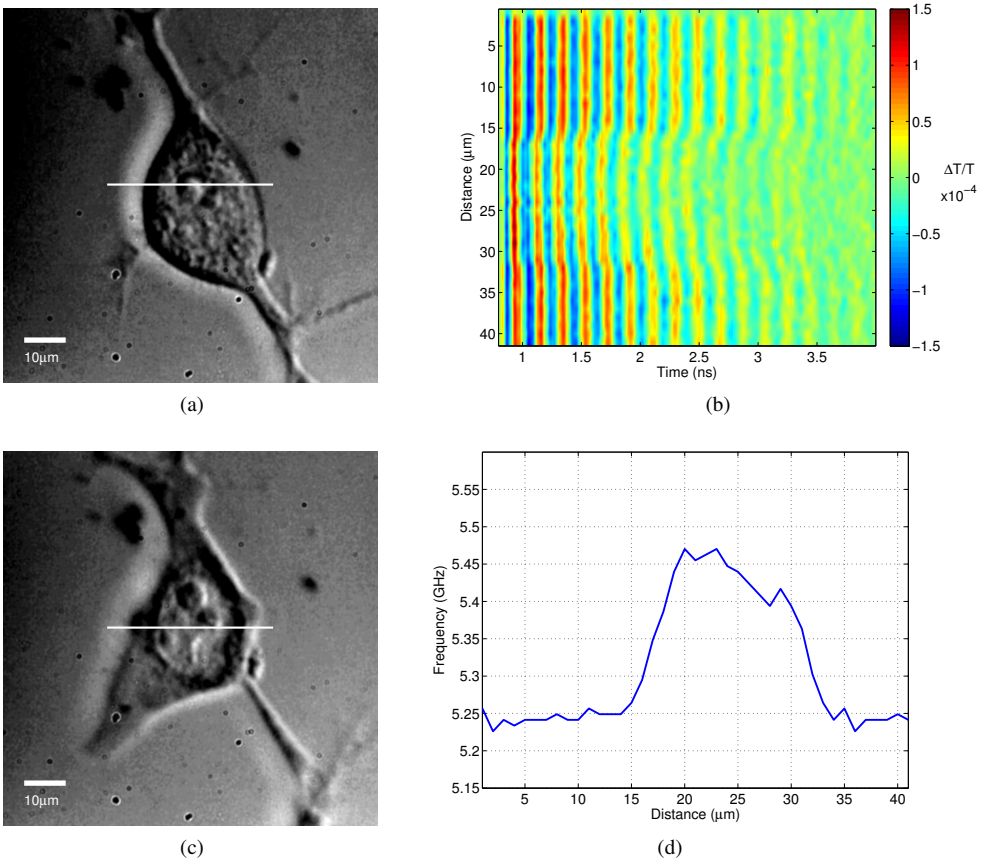

(a) (b) (c) (d)

Fig. 12: Brillouin scanning over living 3T3 cells. Optical picture of the cell before(a) and after (c)the scan. Brillouin frequencies of the white line shown in (a) are shown in (d). (d), B-scan of the Brillouin oscillation in line on (a). The morphology of the cell in (c) after the scan remains structurally intact.

where δt is the transition point in time between one media and the other, f_B is the Brillouin frequency, λ_{probe} is the laser wavelength and n the refractive index of the specimen. Figure 13 shows a b-scan of the phantom cell presented in section 3.3. An estimate of the transition point profile is marked. This delay is proportional to its thickness as seen in equation 2. From the trace in Fig. 9 we can observe a delay of approximately 1.8ns which leads to a calculated thickness of approximately 4μm (equation 2). That result is just under the 5μm nominal size of the polystyrene used to build the phantoms. Since the particles where melted together, this result is reasonable. However, to determine the transition point by computational methods is not a trivial problem and is being currently addressed.

4.2. Acquisition speed

Compared with a mechanical delay line used previously in time-resolved Brillouin measurements, the ASOPS pump probe system gives the opportunity to either have faster scans, more pixels per image or greater SNR through averaging. The pump probe system is fundamentally limited by its delay repetition rate, which is the time required to capture one trace (100 microseconds), and its point-by-point nature. This, in the best case could be fast enough for live

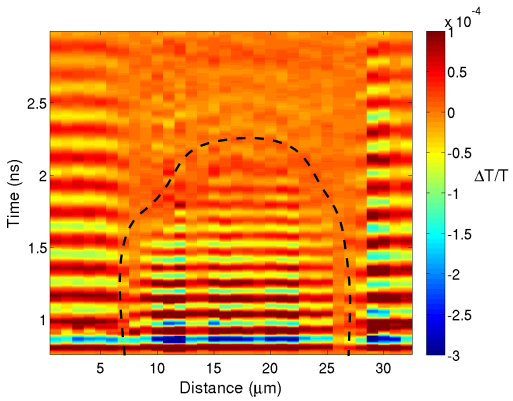

Fig. 13: Bscan scan over phantom cell presented in figure 10.The profile of the phantom is visible from the phantom cell. The black dotted line represents an estimation of the phantom profile.

imaging if; the SNR allows low or no averaging and the system is fast enough to capture all pulses.

Due to technical details in our system, only 1/3 of the available data is used to build a signal leaving the remainder data only to contribute to the stress of the cell. Consequently, it is possible to further reduce radiation exposure by increasing the acquisition system capabilities or by using a pulse picker to block unused pulses when data is not being acquired.

A further increase in speed could be achieved by parallelisation of detection [32] where multiple laser spots are exposed to the sample simultaneously. The speed would be then increased by each extra parallel point. This is a promising way of increasing pump-probe acquisition speeds however, much development is still required.

4.3. Brillouin scattering and future developments of the thin-film transducers

It is unlikely that the refractive index of the cell remains constant; bulk values can be a good approximation for many purposes, but at the scale our imaging is intended to be applied, the variations can not be neglected. To produce accurate speed of sound measurements using Brillouin oscillations it is necessary to have an accurate measure of the refractive index of the specimen within the sampling volume. For that problem, fittings of model data to resolve both refractive index and speed of sound have been applied [17] and we look to use this or any other suitable method to approach this problem.

The transducer resonates and this resonance is detected as shown in section 3. If the cell is well attached to the transducer, it could be possible to observe a variation in the resonance frequency and amplitude related to the damping induced by the cell as presented in *Smith et al* [26]. This could provide useful additional information that is to be explored in the future.

The transducers can be improved by increasing the finesse of the optical cavity, by for instance, replacing ITO for another material with ideally lower losses at λ_{probe} while greater absorption at λ_{pump}. This will improve transmission of λ_{probe} and rejection of λ_{pump} allowing better SNR without increasing the damage induced to the cell. The glass substrate could be replaced with a sapphire one for better heat dissipation.

Cells grown on the transducers exhibited normal attachment and spreading, when coated with standard Poly-L-lysine and ultrasound has been demonstrated to be biocompatible at 1.7GHz [7], however, our implementation using pulsed laser exerts additional potential stressors on

the preparation which bright field imaging is a poor method to evaluate. While morphology and in particular dynamics of the cellular margins provided encouragement with respect to the continued viability of cells during and post-experiment, fluorescence assays will be further applied to screen for cell damage and death during our experiments.

5. Conclusion

In this paper, images and measurements of time-resolved Brillouin oscillations on fixed and living mammalian cells are reported, to our knowledge, for the first time. The measurements, allowed the calculation, based on the Brillouin equation (eq 1), of speed of sound maps of phantom cells (at GHz frequency range). The measurements were performed by the application of multifunctional thin-film opto-acoustic transducers. These structures and measuring system were optimised to address cell fragility enhancing signal-to-noise ratio with respect to incident radiation. This allowed, along with the use of a ASOPS system, the expansion of time-resolved Brillouin oscillations measurements from single point or line to imaging. The flexibility of the transducer was exploited to design a device which can detect Brillouin signals in transmission. This approach is particularly useful, since the transducer serves as a shield to protect the cell from laser pulses and simplifies the detection path. The method was applied to fixed and living cells, which showed good health throughout the experiment. Brillouin frequencies from 5.2 to 5.5GHz were measured when producing Brillouin images from the cultured cells. Calculated sound velocities, assuming homogeneity in refractive index, are 1548 to 1605m/s, which are similar to previously reported results on HeLa cells using SAM (at 0.86GHz) [33] and on vegetal cells using Brillouin oscillations ($\sim$5GHz) [22].